1-1-1988

A Two-Dimensional Mathematical Model of a Porous Lead Dioxide Electrode in a Lead-Acid Cell

E. C. Dimpault-Darcy
Texas A & M University - College Station

T. V. Nguyen
Texas A & M University - College Station

Ralph E. White
University of South Carolina - Columbia, white@cec.sc.edu

Publication Info

Journal of the Electrochemical Society, 1988, pages 278-285.

http://www.electrochem.org
DOI: 10.1149/1.2095601
http://dx.doi.org/10.1149/1.2095601

A Two-Dimensional Mathematical Model of a Porous Lead Dioxide Electrode in a Lead-Acid Cell

E. C. Dimpault-Darcy,* T. V. Nguyen,* and R. E. White**

Department of Chemical Engineering, Texas A&M University, College Station, Texas 77843-3122

ABSTRACT

A two-dimensional mathematical model is presented for a lead dioxide electrode in a lead-acid cell. It is used to simulate the time dependent behavior of the electrode during discharge. The model contains six dependent variables: the concentration of the acid electrolyte, the porosity, the electrical potentials of the solid and solution phases, and the two directional components of the current density in the electrolyte. The effect of the electrode grid was included by varying the conductivity of the solid. Parameters such as electrode conductivity, electrode dimensions, and temperature are investigated to understand their effects on electrode discharge performance.

The combination of low cost, versatility, and excellent rechargeability of the lead-acid battery makes it the single most widely used battery system worldwide. Its applications vary from small sealed cells for consumer use to the large load-leveling systems for electric utilities. To complement the traditional trial-and-error approach, which is expensive and time consuming, mathematical models (1-10) have been developed to provide a better understanding of the cause-and-effect relationships and the phenomena involved. However, all earlier models, being one-dimensional, cannot account for the effects of nonuniformity in the vertical direction along the height of the electrode (see Fig. 1) on the electrode discharge performance. Uneven current density distribution has been known to lead to inefficient use of the porous electrodes and, subsequently, would lower the performance of each cell in a battery.

A number of factors could lead to nonuniform current distribution. In a typical lead-acid cell of a car battery, the distance between current collectors is approximately 3 mm, while the height of the electrodes is close to 100 mm. This aspect ratio elicits doubts whether the current distribution is uniform in the y-direction due to electrical resistance effects, since the tab connections are placed near the center at the top of both electrodes and serve as the source and sink of current. Also, during high discharge rates and after deep discharge cycles, the changing conductivity of the solid electrode material could result in significant nonuniformity in the y-direction. Also, the internal resistance of the electrodes increases with the number of cycles (11). After numerous deep cycles, the reforming of lead dioxide during charge does not reproduce a porous matrix with the exact same structure or electrical properties (11). Therefore, it is the objective of this work to develop a two-dimensional model of a porous lead dioxide electrode that can be used as a tool by battery designers to study electrode performance under conditions where nonuniform current density distribution occurs along the height of the electrode.

Figure 1 shows the six elementary parts of the lead-acid cell. A porous positive (PbO_2) electrode and a porous negative (Pb) electrode, both supported by lead current-collector grids, are separated by a reservoir of electrolyte and a porous separator. The current collectors are situated at the center of each electrode. These elements are repeated alternatively to form a monopolar stack of cells. The thin electrode plates are interleaved such that each positive plate is located between two negative plates.

The porous structure of both electrodes is flooded with a binary aqueous acid electrolyte. Since the bisulfate ion, HSO_4^-, is a rather weak acid, the electrolytic solution consists essentially of three species: H^+, HSO_4^-, and H_2O (the solvent). The electrochemical half reaction at the positive electrode (PbO_2) is

$$PbO_{2(s)} + HSO_4^- + 3H^+ + 2e^- \xrightarrow{\text{discharge}} PbSO_{4(s)} + 2H_2O \quad [I]$$

and the one at the negative electrode (Pb) is

$$Pb_{(s)} + HSO_4^- \xrightarrow{\text{discharge}} PbSO_{4(s)} + H^+ + 2e^- \quad [II]$$

A reservoir of acid electrolyte adjacent to the positive electrode prevents the premature depletion of the acid within the PbO_2 electrode due to reaction [I]. The performance of the positive electrode can be predicted by using a mathematical model for porous electrodes.

The development of the general equations describing the behavior of porous electrodes can be considered to date back to the work of Newman and Tobias (12). Their model and Euler's model (13) deal primarily with current distribution and demonstrate that the polarization equation and the mass transport of the reacting species play a major role in electrode performance. Dunning *et al.* (14) use numerical techniques to include the diffusional transport of the active species within the porous electrodes using a macroscopic approach and apply a Butler-Volmer-type polarization equation.

Simonsson (1) and Micka and Roušar (2-5) concentrate their efforts on the porous electrodes of the lead-acid battery. They use a macro-homogeneous approach to disregard the actual geometric detail of the pores and describe the porous electrodes as a superposition of two continuous phases, liquid and solid. Simonsson predicts that a reaction layer moves inward into the lead dioxide electrode due to gradual insulation of the surface by covering lead sulfate crystals. Micka and Roušar modeled a positive PbO_2 electrode (2, 3) and a negative Pb electrode (4) separately, and afterwards combined the equations to model a complete cell (5). They show that the theoretical discharge capacity of the cell is limited by the positive (PbO_2) electrode at normal temperatures and discharge rates.

A model by Gidaspow and Baker (6) is used to describe the transformation of one solid phase into another in a porous electrode. Their model predicts cell failure by

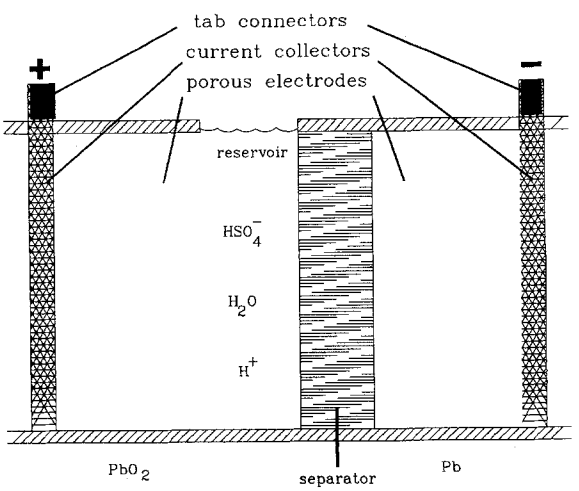

Fig. 1. Schematic of a lead-acid cell

*Electrochemical Society Student Member.
**Electrochemical Society Active Member.

blockage of the pores by lead sulfate deposition. However, they use a linear polarization equation which is valid only at low current densities.

Newman and Tiedemann (7) provide a comprehensive review of the development of porous electrode theory prior to 1975. A material balance equation which includes porosity as a simultaneous variable is presented for the acid electrolyte. Tiedemann and Newman (8) and Sunu (9) apply the theory to develop complete cell models to describe the discharge behavior of a cell. Sunu's model includes the possibility of nonuniform concentration in the electrolyte reservoir, which Tiedemann and Newman (8) omit. Gu *et al.* (10) extend these models to predict cell behavior during cycles of discharge, rest, and charge. The time-dependent model can be used to produce one-dimensional profiles of concentration of acid electrolyte, electrode porosity, electrical potentials of the solid and solution phases, and current density.

A two-dimensional model of the lead-acid cell which contains all the features of the model by Gu *et al.* (10) is not available in the literature. A two-dimensional model by Choi and Yao (15, 16) and a three-dimensional model by Lee *et al.* (17) are strictly thermal models of an individual cell and stacks of cells. These models are for determining temperature profiles to design an optimum electrolyte-circulation process for efficient heat removal in a battery system. Two-dimensional models of a solid electrode by Choi and Yao (18) and of a simple cell configuration with an essentially porous electrode by Nishiki *et al.* (19) show the nonuniformities in the current and potential distributions which occur due to ohmic drop even with simple geometries. This is substantiated by two-dimensional models of current-collector grids by Sunu and Burrows (20, 21), which demonstrate the effect of grid design, tab position, and grid weight on current and potential distributions. However, in these models, the effects of concentration and porosity variations are omitted. The model presented here extends the equations of the Gu *et al.* model (10) to predict the time dependent, two-dimensional variations in concentration, porosity, potentials of solid and solution phases, and two components of the current density.

A finite difference method was chosen to solve the model equations. It consists of a combination of the implicit alternating direction (IAD) method (22) and Newman's Band (J) technique (23) for solving coupled, nonlinear ordinary differential equations. This method, IAD-Newman, can be used to solve coupled, nonlinear partial diffferential equations (24-26).

Model Description

Figure 2 shows a porous solid lead dioxide electrode with a lead current-collector grid. The model domain is the area shaded in with small dots. The dashed line is the model boundary which splits the current collector and electrode at its center to form an axis of symmetry. Hence, the horizontal dimensions of the grid/electrode region, x_{cc}, and the electrode region, x_{th}, are described in terms of half-thicknesses. The solid part of the current collector protruding above the model boundary is the tab connector.

In order to account for the essential features of a porous electrode without going into exact geometric detail, the pore system of the electrode is regarded as a homogeneous macroscopic region with distributed quantities. That is, each node (or dot) in Fig. 2 represents a small volume of solid matrix material with pore-filling electrolyte. This volume element is small with respect to the overall dimensions but large compared to the pore structure. Hence, for this volume element, the potentials in the solid, Φ_1, and in the electrolyte, Φ_2, represent averaged quantities. These variables coincide spatially because the porous electrode outside of the grid is treated as a superposition of two continua, solution and solid.

The current collector is a nonporous lead grid (20, 21) which supports the porous lead dioxide material. This grid is assumed to change the electrical conductivity of the solid matrix in the grid/electrode region (the x_{cc} region in Fig. 2). The size and shape of the lead grid could alter the initial porosity of this region; however, in this study, the initial porosity in the grid/electrode region is assumed to be the same as in the other electrode region ($x_{th} - x_{cc}$ region in Fig. 2), but this condition could easily be relaxed to account for different grid shapes.

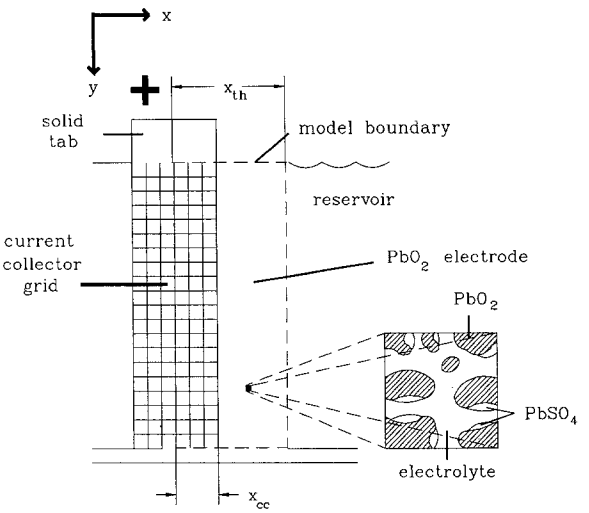

Fig. 2. Schematic of a lead dioxide electrode with the model boundary shown by the dashed line.

To simplify the model, convective flow of the electrolyte is considered negligible which eliminates velocity vectors from the governing equations. The behavior of the electrolyte, which dissociates primarily into H^+ and HSO_4^- in water, is described by binary concentrated solution theory (23). Isothermal conditions are assumed, and the physical, transport, and kinetic parameters are treated as constants.

The independent variables are the two spatial coordinates, x and y, and the discharge time, t. The operating parameters are the specified temperature, T, and the applied current, I. The geometric design parameters are the half-thickness of grid/electrode region, x_{cc}, the half-thickness of the electrode, x_{th} the heights of these, y_h, and the width of the electrode plates, z_w.

The mathematical model consists of six independent governing equations for six dependent variables. The six unknowns are: the concentration of the electrolyte, c, the potential in the solid phase, Φ_1, the potential in the electrolyte, Φ_2, the porosity, ϵ, and the two components of the superficial current density in the electrolyte, $\vec{i}_{2x}$ and $\vec{i}_{2y}$. From these unknowns, four quantities of interest can be calculated for analysis of electrode behavior. These are: the local transfer current per unit volume, j, the state of charge per unit volume, Q, and the two components of the superficial current density in the solid phase, $\vec{i}_{1x}$ and $\vec{i}_{1y}$.

The equations describing the physical phenomena occurring in the porous lead dioxide electrode during discharge are extensions of those presented earlier (1):

Material balance.—

$$\epsilon \frac{\partial c}{\partial t} - \epsilon^{ex} D \nabla^2 c - ex\epsilon^{ex-1} D(\nabla \epsilon \cdot \nabla c) + \frac{1}{2F}\left[\left(\frac{MW_{PbSO_4}}{\rho_{PbSO_4}} - \frac{MW_{PbO_2}}{\rho_{PbO_2}}\right) c + 2t^\circ_+ - 3\right] \nabla \cdot \vec{i}_2 = 0 \quad [1]$$

Porosity balance.—

$$\frac{\partial \epsilon}{\partial t} - \frac{1}{2F}\left(\frac{MW_{PbSO_4}}{\rho_{PbSO_4}} - \frac{MW_{PbSO_2}}{\rho_{PbO_2}}\right) \nabla \cdot \vec{i}_2 = 0 \quad [2]$$

Divergence of current.—

$$\nabla \cdot \vec{i}_2 - \nabla \cdot (\sigma_s \epsilon^{exm} \nabla \Phi_1) = 0 \quad [3]$$

Ohm's law in solution.—

$$\frac{\vec{i}_2}{\kappa \epsilon^{ex}} + \nabla \Phi_2 - \frac{RT}{F}\left[\frac{3 - 2t^\circ_+}{c} + \frac{2V_o}{1 - cV_e}\right] \nabla c = 0 \quad [4]$$

Electrode kinetics.—

$$\nabla \cdot \vec{i}_2 - a_{max} i_{o,ref} \left(\frac{c}{c_{ref}}\right)^{\gamma} \left(\frac{\epsilon - \epsilon_o}{\epsilon_{max} - \epsilon_o}\right)^{\zeta} \left\{\exp\left[\frac{a_a \mathbf{F}}{RT}(\Phi_1 - \Phi_2)\right] - \exp\left[-\frac{a_c \mathbf{F}}{RT}(\Phi_1 - \Phi_2)\right]\right\} = 0 \quad [5]$$

Equation [1] states that the electrolyte concentration at any point in the electrode changes with time due to diffusion and electrode reaction. In Eq. [2], the conversion of active material due to electrode reaction dictates the change in porosity with time. Equation [3], a charge balance, states that the divergence of the total current density within the electrode must equal zero. In the electrolyte, the gradients in potential and in chemical potential determine the current density according to Eq. [4]. Finally, Eq. [5] governs the kinetics of the electrode reaction. The development of these equations is discussed by Dimpault-Darcy (27).

Note that the terms of Eq. [4] are vector terms and not scalar terms like in the other equations. Consequently, for two-dimensional analysis, Eq. [4] is split into an x-component equation

$$\frac{\vec{i}_{2x}}{\kappa \epsilon^{ex}} + \frac{\partial \Phi_2}{\partial x} - \frac{RT}{\mathbf{F}}\left[\frac{3 - 2t^{\circ}_{+}}{c} + \frac{2V_o}{1 - cV_e}\right]\frac{\partial c}{\partial x} = 0 \quad [4x]$$

and a y-component equation

$$\frac{\vec{i}_{2x}}{\kappa \epsilon^{ex}} + \frac{\partial \Phi_2}{\partial y} - \frac{RT}{\mathbf{F}}\left[\frac{3 - 2t^{\circ}_{+}}{c} + \frac{2V_o}{1 - cV_e}\right]\frac{\partial c}{\partial y} = 0 \quad [4y]$$

Hence, for the finite difference formulation of these equations and boundary conditions, there are six equations with six unknowns at each node.

Initially, the concentration of the electrolyte and the porosity of the matrix can be set at any value. The initial concentration is labeled c_{res}, and the initial porosity, ϵ_{max}. The other variables do not require initial values.

An overview of the boundary conditions is given next (more details are presented in the Numerical Solution Technique Section). A choice of boundary conditions was made to simulate the conditions imposed by the neighboring components of the PbO_2 electrode in a lead-acid cell during discharge. For this two-dimensional model, the four boundaries are referred to as the center boundary for the center of the electrode, as the reservoir boundary for the electrode/reservoir interface, and as the upper and lower boundary for the top and bottom of the electrode, respectively.

The material balance equation is second order with respect to its derivatives. Consequently, two boundary conditions per spatial dimension are needed to obtain a particular solution. At the reservoir boundary, the concentration is maintained at

$$c = c_{res} \quad \text{at} \quad x = x_{th} \quad \text{for all } y \quad [6]$$

while at the center boundary, symmetry principles yield

$$\frac{\partial c}{\partial x} = 0 \quad \text{at} \quad x = 0 \quad \text{for all } y \quad [7]$$

At the upper and lower boundaries, the condition

$$\frac{\partial c}{\partial y} = 0 \quad \text{at} \quad y = 0 \quad \text{and} \quad y = y_h \quad \text{for all } x \quad [8]$$

applies since they are treated as insulated boundaries.

No boundary condition is required for the variable ϵ, and Eq. [2] applies everywhere. The potential conditions at the center boundary are

$$\frac{\partial \Phi_1}{\partial x} = 0 \quad \text{at} \quad x = 0 \quad \text{for all } y \quad [9]$$

$$\frac{\partial \Phi_2}{\partial x} = 0 \quad \text{at} \quad x = 0 \quad \text{for all } y \quad [10]$$

according to symmetry principles. At the reservoir boundary, the potential in the electrolyte is set at

$$\Phi_2 = \Phi_{2,res} \quad \text{at} \quad x = x_{th} \quad \text{for all } y \quad [11]$$

which is analogous to Eq. [6]. Equation [5] applies for Φ_1 at the reservoir and lower boundary. Since the electrolyte is bounded at the upper and lower boundaries

$$\frac{\partial \Phi_2}{\partial y} = 0 \quad \text{at} \quad y = 0 \quad \text{and} \quad y = y_h \quad \text{for all } x \quad [12]$$

is the condition at the top and bottom for Φ_2.

At the top of the electrode, a tab connector serves as a sink of current during discharge. For the part of the upper boundary in contact with the tab, the condition is

$$\frac{\partial \Phi_1}{\partial y} = -\frac{I}{\sigma_{cc} x_{cc} z_w} \quad \text{for} \quad 0 \le x \le x_{cc} \quad \text{at} \quad y = 0 \quad [13]$$

and for the part not in contact with the tab, the condition is

$$\frac{\partial \Phi_1}{\partial y} = 0 \quad \begin{cases} \text{for } x_{cc} < x \le x_{th} \text{ at } y = 0 \\ \text{for } 0 \le x \le x_{th} \text{ at } y = y_h \end{cases} \quad [14]$$

which also applies for the bottom boundary.

Current enters the electrode matrix at the reservoir boundary in the electrolyte according to the condition

$$\vec{i}_{2x} = \frac{I}{y_h z_w} \quad \text{at} \quad x = x_{th} \quad \text{for all } y \quad [15]$$

At this boundary, all the current density is in the x-direction, since the gradients in Eq. [4y] are zero due to Eq. [6] and [11], which leaves

$$\vec{i}_{2y} = 0 \quad \text{at} \quad x = x_{th} \quad \text{for all } y \quad [16]$$

as the other condition for the current density. At the center boundary, the current has shifted to be parallel to the y-direction, resulting in

$$\vec{i}_{2x} = 0 \quad \text{at} \quad x = 0 \quad \text{for all } y \quad [17]$$

For the upper and lower boundaries

$$\vec{i}_{2y} = 0 \quad \text{at} \quad y = 0 \quad \text{and} \quad y = y_h \quad \text{for all } x \quad [18]$$

applies since the electrolyte is bounded there. The current parallel to the top and bottom, $\vec{i}_{2x}$, is governed by Eq. [4x], and similarly, Eq. [4y] applies for $\vec{i}_{2y}$ at the center boundary.

Table I. Grid diagrams for the implementation of IAD-Newman method

a. Implicit in the x-direction

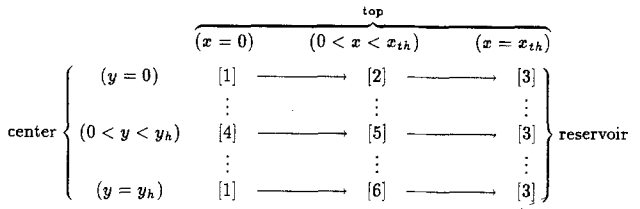

b. Implicit in the y-direction

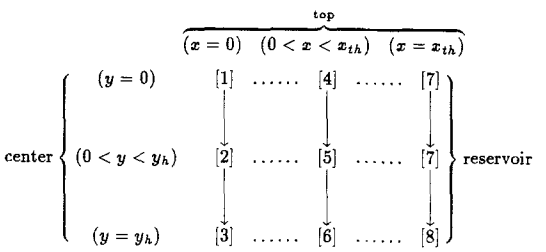

Numerical Solution Technique

The finite difference method used consists of a combination of the implicit alternating-direction (IAD) method (22) and Newman's Band (J) technique (23) for solving coupled, nonlinear ordinary differential equations. This method, IAD-Newman, can be used to solve coupled, nonlinear partial differential equations (24-26).

All spatial derivatives in the equations are approximated with three point difference approximations which are accurate to $O(h^2)$, where h represents the spatial distance between nodes (either Δx or Δy). As with all numerical solutions of time dependent problems, the accuracy of the results depends also on the time step size, Δt. Two-significant-digit accuracy in the resulting solutions was achieved by adding more nodal points in both directions and reducing the time step until there was no change in the second digit. With a convergence criterion which required four to five iterations and using 21 nodes in both directions, each time step took an average of nearly 1 min of CPU time on a DEC VAX 8800.

The IAD-Newman technique splits every time step into two half-time steps, $\Delta t/2$. During the first half-time step, all model equations (including boundary conditions) are solved implicitly in one direction (x), and during the following half-time step, they are solved in the other direction (y). The intermediate values of the variables obtained from solving the first step (labeled with a superscript *) are subsequently used in the second step in solving for the solution values after a full time step.

The grid diagram shown in Table Ia illustrates how the first half-time step is implemented. The model equations and boundary equations used at each numbered location are listed in Table II. The grid diagram in Table Ib is for the second half-time step. The equations and boundary conditions are listed in Table III. Note that at positions [3] and [6], the condition, $\Phi_2 = \Phi^*_2$, was used instead of the condition listed previously in Eq. [12]. This Dirichlet condition was necessary to obtain a particular solution (25, 26). It states that the potential does not change during that half-time step. The Neumann condition desired at the bottom boundary is substituted in the formulation of the governing equations for the first half-time step. However, a solution to the equations could not be attained with this condition implemented in the second half-time step.

Table II. Model equations solved in the x-direction

[1]	[2]	[3]
$\partial c/\partial x = 0$	Eq. [1]	$c = c_{res}$
Eq. [2]	Eq. [2]	Eq. [2]
$\partial\Phi_2/\partial x = 0$	Eq. [3]	$\Phi_2 = \Phi_{2,res}$
$\vec{i}_{2x} = 0$	Eq. [4x]	$\vec{i}_{2x} = I/y_h z_w$
$\vec{i}_{2y} = 0$	$\vec{i}_{2y} = 0$	$\vec{i}_{2y} = 0$
$\partial\Phi_1/\partial x = 0$	Eq. [5]	Eq. [5]
[4]	[5]	[3]
$\partial c/\partial x = 0$	Eq. [1]	$c = c_{res}$
Eq. [2]	Eq. [2]	Eq. [2]
$\partial\Phi_2/\partial x = 0$	Eq. [3]	$\Phi_2 = \Phi_{2,res}$
$\vec{i}_{2x} = 0$	Eq. [4x]	$\vec{i}_{2x} = I/y_h z_w$
Eq. [4y]	Eq. [4y]	$\vec{i}_{2y} = 0$
$\partial\Phi_1/\partial x = 0$	Eq. [5]	Eq. [5]
[1]	[6]	[3]
$\partial c/\partial x = 0$	Eq. [1]	$c = c_{res}$
Eq. [2]	Eq. [2]	Eq. [2]
$\partial\Phi_2/\partial x = 0$	Eq. [3]	$\Phi_2 = \Phi_{2,res}$
$\vec{i}_{2x} = 0$	Eq. [4x]	$\vec{i}_{2x} = I/y_h z_w$
$\vec{i}_{2y} = 0$	$\vec{i}_{2y} = 0$	$\vec{i}_{2y} = 0$
$\partial\Phi_1/\partial x = 0$	Eq. [5]	Eq. [5]

Results and Discussion

The utility of the model in simulating the behavior of a lead dioxide electrode in a lead-acid cell is determined by analyzing the results produced under various conditions. Rather than studying all possible parameters and operating conditions, which would be an overwhelming task, a few important case studies are presented to exhibit the model predictions of the discharge behavior of a lead dioxide electrode. The model is used here to produce two-dimensional profiles of the concentration of the electrolyte (c), the overpotential (η), and the potential drop across the electrode thickness

$$\eta_{PbO_2} = \Phi_1(0,y) - \Phi_2(x_{th},y) \quad [19]$$

Table III. Model equations solved in the y-direction

[1]	[4]	[7]
$\partial c/\partial y = 0$	$\partial c/\partial y = 0$	$c = c_{res}$
Eq. [2]	Eq. [2]	Eq. [2]
$\partial\Phi_2/\partial y = 0$	$\partial\Phi_2/\partial y = 0$	$\Phi_2 = \Phi_{2,res}$
$\vec{i}_{2x} = 0$	Eq. [4x]	$\vec{i}_{2x} = I/y_h z_w$
$\vec{i}_{2y} = 0$	$\vec{i}_{2y} = 0$	$\vec{i}_{2y} = 0$
$\partial\Phi_1/\partial x = -I/(\sigma_{cc} x_{cc} z_w)$	$\partial\Phi_1/\partial x = -I/(\sigma_{cc} x_{cc} z_w)$ or $(= 0)$	Eq. [5]
[2]	[5]	[7]
Eq. [1]	Eq. [1]	$c = c_{res}$
Eq. [2]	Eq. [2]	Eq. [2]
Eq. [3]	Eq. [3]	$\Phi_2 = \Phi_{2,res}$
$\vec{i}_{2x} = 0$	Eq. [4x]	$\vec{i}_{2x} = I/y_h z_w$
Eq. [4y]	Eq. [4y]	$\vec{i}_{2y} = 0$
Eq. [5]	Eq. [5]	Eq. [5]
[3]	[6]	[8]
$\partial c/\partial y = 0$	$\partial c/\partial y = 0$	$c = c_{res}$
Eq. [2]	Eq. [2]	Eq. [2]
$\Phi_2 = \Phi^*_2$	$\Phi_2 = \Phi^*_2$	$\Phi_2 = \Phi_{2,res}$
$\vec{i}_{2x} = 0$	Eq. [4x]	$\vec{i}_{2x} = I/y_h z_w$
$\vec{i}_{2y} = 0$	$\vec{i}_{2y} = 0$	$\vec{i}_{2y} = 0$
Eq. [5]	Eq. [5]	$\partial\Phi_1/\partial x = 0$

Table IV. Parameter values studied

Parameter	Symbol	Value
Half-thickness of porous electrode	x_{th}	0.10 or 0.05 cm
Initial acid concentration	c_{res}	0.0049 mol/cm^3 *
Conductivity of grid/electrode region	σ_{cc}	48000 or 4800 S/cm
Temperature	T	300 or 250 K

* Also varied linearly with y from 0.0049 to 0.0039 mol/cm^3

The independent parameters investigated were the half-thickness of the porous electrode (x_{th}), the conductivity of the grid/electrode region (σ_{cc}), and the temperature (T). The initial acid concentration (c_{res}), which is also the concentration maintained at the reservoir boundary during discharge, was varied to study the effects of concentration gradients due to an unmixed reservoir. The values of each parameter tested are listed in Table IV.

The discharge behavior of a lead dioxide electrode at a constant applied current of −22.5A and at 300 K is presented first. The current corresponds to a current density of −300 mA/cm^2 entering the electrode at the reservoir interface. The electrode half-thickness (x_{th}) was set at 0.1 cm, and the half-thickness of the grid/electrode region (x_{cc}) was set at 0.05 cm. Using values from Bode (2), the conductivity of the grid/electrode region, σ_{cc}, was set to be one order magnitude greater than the conductivity of the lead dioxide region (σ_{PbO_2}). The other parameters are given in Table V.

Figure 3 shows the distributions of concentration in the electrode after a 60s discharge. The concentration of the acid is reduced due to the electrode reaction since diffusion from the reservoir is not rapid enough to maintain c at c_{res} in the entire electrode. Note that concentration gradients in the y-direction are negligible during the discharge of the electrode. The reason may be due to the fact that the initial porosity distributions in the electrode were assumed to be uniform; although, in reality it is very likely that they are not. Nonuniform porosity distribution gives rise to nonuniform electrode conductivity and unequal diffusion rate of the acid. Additionally, nonuniform porosity distribution may occur upon cycling. This effect has been observed experimentally (11) and has been demonstrated by the work of Gu *et al.* (10), in which it was illustrated that during discharge followed by rest and charge and depending on the operating temperature the porosity distribution is not fully recovered to the original distribution. Also, to examine whether or not greater depth of discharge would result in nonuniformities, the electrode was discharged for 120s, and it was found that the two-dimensional effects were still minimal as expected because of the uniform, initial conditions employed.

Table V. Parameter values held fixed

Parameter (reference number)	Symbol	Value
Acid Electrolyte conductivity at 25 °C (2)	κ_{25}	0.79 S/cm
Acid diffusion coefficient at 25 °C (16)	D_{25}	3.2 x 10^{-5} cm^2/s
Applied current	I	−22.5 A *
Anodic transfer coefficient (16)	α_a	0.5
Cathodic transfer coefficient	α_c	1.5
Density of lead-sulfate	ρ_{PbSO_4}	6.3 g/cm^3
Density of lead-dioxide	ρ_{PbO_2}	9.7 g/cm^3
Exchange current density at c_{ref}	$i_{o,ref}$	0.002 A/cm^2
Exponent for concentration dependence of i_o	γ	1.5
Exponent for deposition coverage (16)	ζ	1.0
Exponent for tortuosity of pore system	ex	1.5
Exponent for tortuosity of solid matrix	exm	0.5
Half-thickness of current collector	x_{cc}	0.05 cm
Height of electrode	y_h	10.0 cm
Lead dioxide conductivity	σ_{PbO_2}	4800 S/cm
Maximum porosity	ϵ_{max}	0.50
Maximum specific surface area	a_{max}	100 cm^2/cm^3
Partial molar volume for the electrolyte (2)	$\bar{V}_e$	45.0 cm^3/mol
Partial molar volume for the solvent (2)	$\bar{V}_o$	17.5 cm^3/mol
Reference concentration of the electrolyte (16)	c_{ref}	0.0049 mol/cm^3
Time step	Δt	0.1 s
Transference number (2)	t_+^o	0.72
Width of the electrode plates	z_w	7.5 cm

* Current is negative because it flows in the negative x-direction into the PbO_2 electrode from the reservoir and in the negative y-direction out of the PbO_2 electrode into the tab (see Fig. 2)

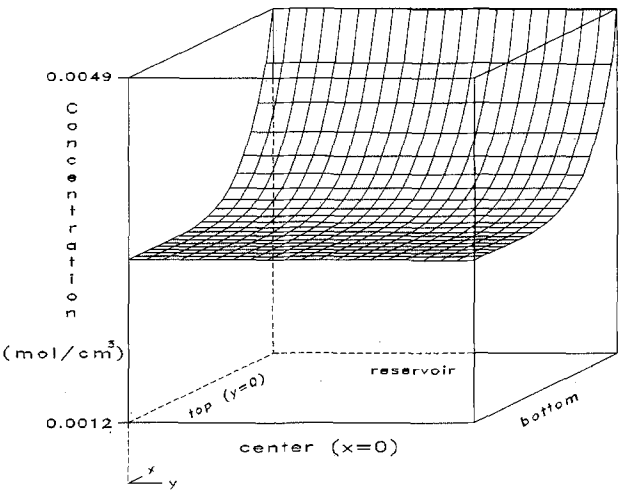

Fig. 3. Concentration distribution after 60s discharge (x_{cc} = 0.05 cm, x_{th} = 0.10 cm, σ_{cc} 48,000 S/cm, and σ_{PbO_2} = 4800 S/cm).

In Fig. 4, the distribution of the overpotential, as defined by

$$\eta = \Phi_1 - \Phi_2 \qquad [20]$$

shows that the absolute value of overpotential is higher near the reservoir boundary. Note that the viewpoint of the plot has been rotated for a clearer view of the contour. Due to the high conductivity of the solid, the gradients of Φ_1 are small (Eq. [3]). Consequently, changes in overpotential are due mostly to variations in the electrolyte potential, Φ_2. Near the reservoir boundary, most of the applied current density exists in the solution

$$\vec{i}_{2x} \cong \frac{I}{y_h z_w} \quad \text{and} \quad \vec{i}_{1x}, \vec{i}_{1y} \cong 0 \qquad [21]$$

Therefore, the electrolyte potential and concentration gradients are highest there (Eq. [4x]). However, under these conditions the electrolyte potential gradients in the y-direction are not sufficient to produce a significant current, $\vec{i}_{2y}$, in that direction. This explains the uniform concentration with respect to the y-direction.

In Fig. 5, the electrode potential (η_{PbO_2}), as defined in Eq. [19], is shown to have a nearly planar contour relative to the

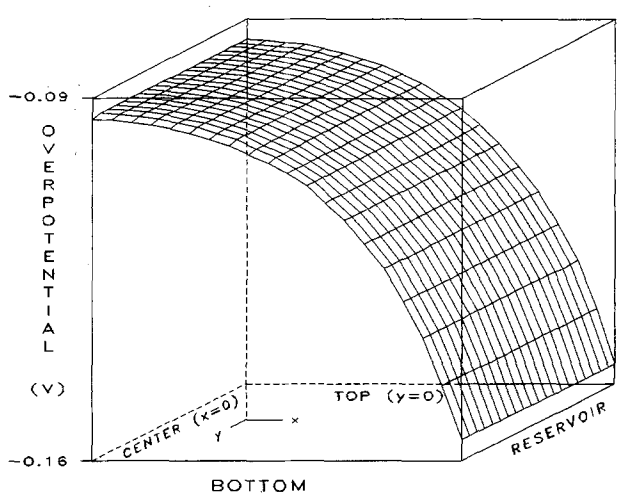

Fig. 4. Overpotential distribution after 60s discharge (x_{cc} = 0.05 cm, x_{th} = 0.10 cm, σ_{cc} = 48,000 S/cm, and σ_{PbO_2} = 4800 S/cm).

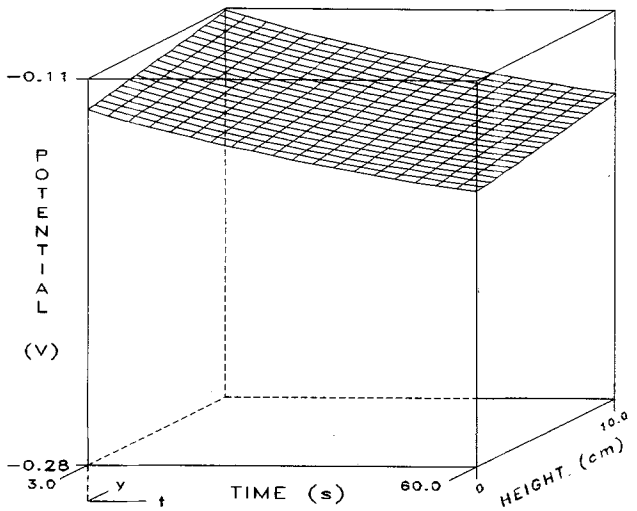

Fig. 5. Electrode potential vs. time and height (x_{cc} = 0.05 cm, x_{th} = 0.10 cm, σ_{cc} = 48,000 S/cm, and σ_{PbO_2} = 4800 S/cm).

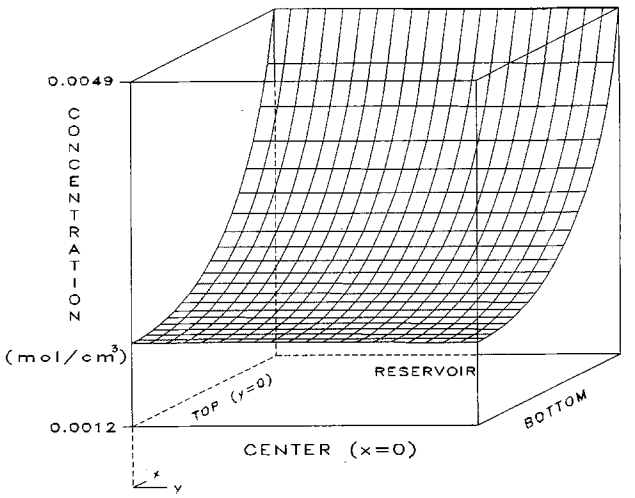

Fig. 7. Concentration distribution after 60s discharge (x_{cc} = x_{th} = 0.05 cm and σ_{cc} = 48,000 S/cm).

time of discharge and the vertical position. The electrode potential decreases with time due to electrode polarization. The electrical resistance of the electrode material contributes to the voltage drop from the bottom to the top of the electrode. Remember, that current flows up to the tab connector at the top boundary (y = 0) during discharge.

To determine the effect the conductivity of the solid Pb in the grid has on electrode behavior, σ_{cc} was set equal to σ_{PbO_2}. The electrode potential profile *vs.* time and y-position in Fig. 6 is steeper than in Fig. 5 due to the reduced conductivity of the grid/PbO_2 region. The result of reducing σ_{cc} by an order of magnitude is a twofold increase in the absolute value of the minimum electrode potential. However, with such conductivities, and even with much lower values (≅100 S/cm), the previously presented profiles are essentially unchanged. With the electrode dimensions studied, the ohmic losses due to the solid play a less crucial role in the performance of the electrode than losses due to the electrolyte because the solid conductivity is much greater than the electrolyte conductivity.

In the manufacturing process of porous lead dioxide electrode plates, an expanded lead grid is coated with a "paste" of PbO_2 which adheres to the grid (28). The paste can be constructed to extend beyond the volume of the grid, which is called overpasting (29). As shown in Fig. 2, a typical range of overpasting has the paste extended beyond the grid by about 50% of the thickness of the grid (29). Conversely, the paste can be constructed with the paste as flush as possible along the sides of the grid, which results in minimum overpasting (29).

In the previous analysis, the half-thicknesses of the porous electrode matrix, x_{th}, and current collector grid, x_{cc}, are 0.1 and 0.05 cm, corresponding to maximum overpasting. For comparison, an electrode with minimum overpasting is examined next by using the same grid dimensions and making x_{cc} = x_{th} = 0.05 cm. The resulting electrode is smaller and contains only one region. In this comparison, the conductivity of the grid/electrode region is the same as previously (*i.e.*, σ_{cc} = 48,000 S/cm). Figure 7 shows the distribution of concentration in the electrode after 60s of discharge for this case. The profile should be compared to Fig. 3, and is similar in contour except that the depletion of acid concentration at the center boundary is more pronounced. This is because the same current is drawn from a smaller electrode.

The next independent variable considered is temperature. The electrolyte conductivity and diffusion coefficient depend on temperature according to (10)

$$\kappa = \kappa_{25} \exp\left(\frac{1801}{298.15} - \frac{1801}{T}\right) \quad [22]$$

$$D = D_{25} \exp\left(\frac{2174}{298.15} - \frac{2174}{T}\right) \quad [23]$$

where κ and D are the conductivity and the diffusion coefficient of 1.280 sp gr H_2SO_4 at the absolute temperature, T. The conductivity and diffusion coefficient at 25°C are κ_{25} and D_{25}. The temperature dependence of other parameters such as the exchange current density and the conductivities of the solids were not included in the model.

The profile of concentration after a minute of discharge at 250 K (−23°C) is shown in Fig. 8. In comparison to Fig. 7,

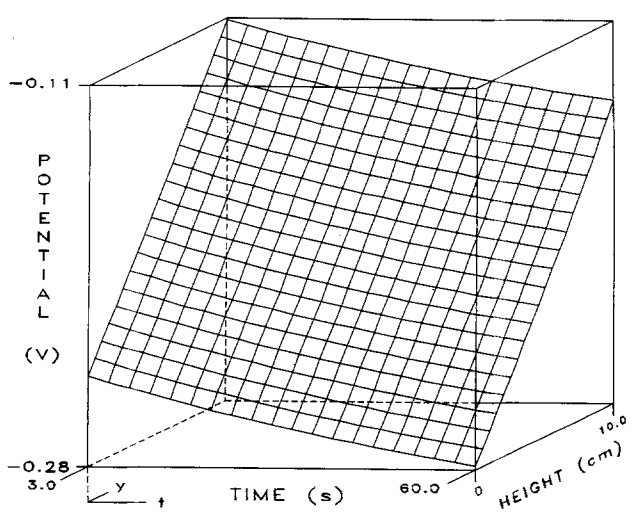

Fig. 6. Electrode potential vs. time and height (x_{cc} = 0.05 cm, x_{th} = 0.10 cm, and σ_{cc} = σ_{PbO_2} = 4800 S/cm).

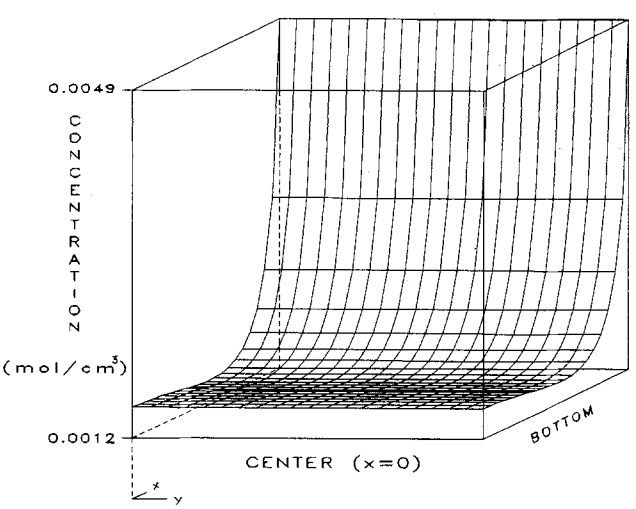

Fig. 8. Concentration distribution after 60s discharge (x_{cc} = x_{th} = 0.05 cm, σ_{cc} = 48,000 S/cm, and T = 250 K).

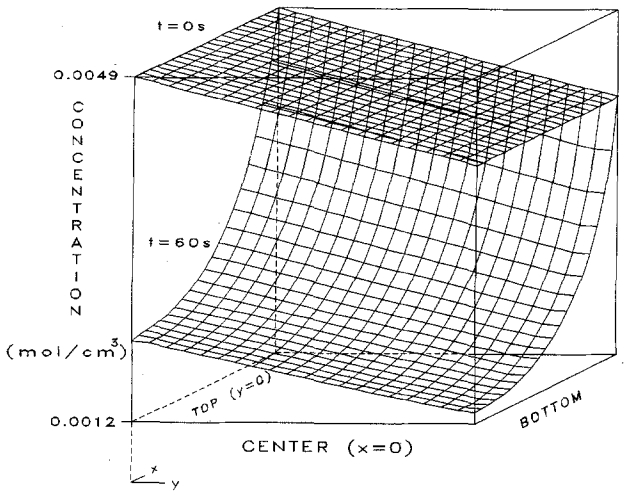

Fig. 9. Concentration distribution after 60s discharge beginning with a nonuniform initial profile ($x_{cc} = x_{th} = 0.05$ cm, and $\sigma_{cc} = 48{,}000$ S/cm).

the concentration gradients are steeper at the lower temperature. The slower diffusion at the lower temperature retards the acid electrolyte transport to the acid depleted center boundary. The minimum shifts to the middle of the electrode because the reduced porosity at the reservoir boundary impedes the acid transport.

The previous results indicate that changes in the dependent variables are small in the y-direction relative to variations in the x-direction. Since a two-dimensional model of a complete cell has not been generated, it would be premature to conclude that such a model would yield predictions with the same uniformity. Simulating discharge under nonuniform initial and boundary conditions produces results which indicate the electrode's behavior to gradients caused possibly by the other cell components, such as the reservoir or the separator. For example, nonuniform acid concentration in the reservoir occurs as a result of density stratification due to gravity during discharge and nonuniform reaction rate in the electrode.

Introducing an initial gradient in concentration in the electrode and maintaining it at the reservoir resulted in the concentration profiles shown in Fig. 9. The initial profile is superimposed over the profile after 60s of discharge for immediate comparison. The initial concentration was set with a linear gradient along the height of the electrode which was maintained at the reservoir boundary as $c_{res}(y)$. For this case study, the difference between the top and bottom concentrations along the reservoir boundary was 20%. The physical representation of this boundary condition is difficult to justify in the presence of diffusion along the boundary, but it demonstrates the model sensitivity to nonuniform conditions in the y-direction. After 60s, the gradient introduced in the reservoir induced a 35% difference in between the top and bottom concentration at the centerline. Figure 9 demonstrates that the model can be used to predict significant gradients in the y-direction when nonuniform boundary conditions are used.

Conclusions and Recommendations

The model presented here has been shown to be capable of predicting the discharge behavior of a porous PbO_2 electrode in two dimensions. The model predictions can be used to promote a cause and effect understanding of the complex time-dependent phenomena. The model provides a basis for building two-dimensional models of other electrodes and cells since the equations are fundamental to porous electrode modeling.

The model predictions should be compared to experimental data. Then, the model should be coupled with a negative porous Pb electrode model with a separator to produce a complete cell model to determine the degree of nonuniformity parallel to the electrode surfaces under cell conditions. Predictions of cycles of discharge, rest, and charge could be included by altering the kinetic equation to handle charge (Eq. [10b] in Ref. (10)). In addition, the significance of assuming that the convective flow is negligible should be reconsidered for a complete cell model.

Manuscript submitted March 9, 1987; revised manuscript received *ca.* July 28, 1987.

Texas A&M University assisted in meeting the publication costs of this article.

LIST OF SYMBOLS

a_{max}	maximum specific electroactive interfacial area, cm^{-1}
c	concentration of the binary (H^+ and HSO_4^-) electrolyte, mol/cm^3
c_{ref}	reference concentration of the binary electrolyte, mol/cm^3
c_{res}	concentration of the binary electrolyte at the reservoir, mol/cm^3
D	diffusion coefficient of the binary electrolyte, cm^2/s
D_{25}	diffusion coefficient of the binary electrolyte at 25°C, cm^2/s
ex	tortuosity factor used in Eq. [1] and [4]
exm	tortuosity factor used in Eq. [3]
$\mathbf{F}$	Faraday's constant, 96,487 C/mol of electrons
h	finite spatial stepping distance in finite difference algorithm, cm
$i_{o,ref}$	exchange current density at c_{ref}, A/cm^2
$\vec{i}_1$	superficial current density in the matrix phase, A/cm^2
$\vec{i}_2$	superficial current density in the solution phase, A/cm^2
I	applied current, A
j	local transfer current per unit volume, A/cm^3 ($j = \nabla \cdot i_2$)
MW_i	molecular weight of species i, g/mol
R	universal gas constant, 8.3143 J/mol · K
t	time, s
t°_+	transference number of H^+ relative to velocity of solvent
T	absolute temperature, K
$\bar{V}_e$	partial molar volume of the electrolyte, cm^3/mol
$\bar{V}_o$	partial molar volume of the solvent, cm^3/mol
x	horizontal distance, cm
x_{cc}	half-thickness of the grid/electrode region, cm
x_{th}	half-thickness of the electrode, cm
y	vertical distance, cm
y_h	height of the electrode, cm
z_w	width of the electrode plate, cm

Greek Symbols

α_a	transfer coefficient in the anodic direction
α_c	transfer coefficient in the cathodic direction
γ	exponent for the concentration dependence of the exchange current density
Δt	finite time step in finite difference algorithm, s
Δx	finite stepping distance in x-direction, cm
Δy	finite stepping distance in y-direction, cm
ϵ	porosity or void volume fraction of solid
ϵ_o	electrochemical limiting porosity or final discharge porosity
ϵ_{max}	maximum porosity of solid
ζ	exponent for the porosity dependence of the active interfacial area
η	overpotential, V
η_{PbO_2}	lead dioxide electrode potential, V
κ	conductivity of the solution, $\Omega^{-1}cm^{-1}$
κ_{eff}	effective conductivity of the solution, $\Omega^{-1}cm^{-1}$
κ_{25}	conductivity of the solution at 25°C, $\Omega^{-1}cm^{-1}$
ρ_i	density of a solid phase of species i, g/cm^3
σ_{cc}	conductivity of the grid/electrode region, S/cm
σ_{PbO_2}	conductivity of the PbO_2 matrix, S/cm
σ_s	conductivity of the solid, S/cm
Φ_1	potential in the solid matrix, V
Φ_2	potential in the solution, V
$\Phi_{2,res}$	potential in the solution at the reservoir, V

Subscripts

e	electrolyte
o	solvent
+	cation
1	solid matrix phase
2	electrolyte phase
x	horizontal direction normal to the electrode/reservoir interface

y vertical direction parallel to the electrode/reservoir interface

REFERENCES

1. D. Simonsson, *This Journal*, **120**, 151 (1973).
2. K. Micka and I. Roušar, *Electrochim. Acta*, **18**, 629 (1973).
3. K. Micka and I. Roušar, *Collect. Czech. Chem. Commun.*, **40**, 921 (1975).
4. K. Micka and I. Roušar, *Electrochim. Acta*, **19**, 499 (1974).
5. K. Micka and I. Roušar, *ibid.*, **21**, 599 (1976).
6. D. Gidaspow and B. S. Baker, *This Journal*, **120**, 1005 (1973).
7. J. Newman and W. Tiedemann, *AIChE J.*, **21**, 25 (1975).
8. W. H. Tiedemann and J. Newman, in "Battery Design and Optimization," S. Gross, Editor, p. 23, The Electrochemical Society Softbound Proceedings Series, PV 79-1, Princeton, NJ (1979).
9. W. S. Sunu, in "Electrochemical Cell Design," R. E. White, Editor, p. 357, Plenum Press, New York, (1984).
10. H. Gu, T. V. Nguyen, and R. E. White, *This Journal*, **134**, 2953 (1987).
11. H. Bode, "Lead-Acid Batteries," J. Wiley & Sons, New York, (1977).
12. J. S. Newman and C. W. Tobias, *This Journal*, **109**, 1183 (1962).
13. K. J. Euler, *Electrochim. Acta*, **13**, 1533 (1968).
14. J. S. Dunning, D. N. Bennion, and J. S. Newman, *This Journal*, **118**, 1251 (1971).
15. K. W. Choi and N. P. Yao, *ibid.*, **125**, 1011 (1978).
16. K. W. Choi and N. P. Yao, *ibid.*, **126**, 1321 (1979).
17. J. Lee, K. W. Choi, N. P. Yao, and C. C. Christianson, *ibid.*, **133**, 1286 (1986).
18. K. W. Choi and N. P. Yao, in "Battery Design and Optimization," S. Gross, Editor, p. 51, The Electrochemical Society Softbound Proceedings Series, PV 79-1, Princeton, NJ (1979).
19. Y. Nishiki, K. Aoki, K. Tokuda, and H. Matsuda, *J. Appl. Electrochem.*, **16**, 291 (1986).
20. W. G. Sunu and B. W. Burrows, *This Journal*, **129**, 688 (1982).
21. W. G. Sunu and B. W. Burrows, *ibid.*, **131**, 1 (1984).
22. B. Carnahan, H. A. Luther, and J. O. Wilkes, "Applied Numerical Methods," J. Wiley & Sons, New York (1969).
23. J. S. Newman, "Electrochemical Systems," Prentice-Hall, Inc., Englewood Cliffs, NJ (1973).
24. J. Van Zee, M. A. Edmund, and R. E. White, *Ind. Eng. Chem. Fund.*, **19**, 438 (1980).
25. T. V. Nguyen, C. W. Walton, R. E. White, and J. Van Zee, *This Journal*, **133**, 81 (1986).
26. T. V. Nguyen, C. W. Walton, and R. E. White, *ibid.*, **133**, 1130 (1986).
27. E. C. Dimpault-Darcy, M.S. Thesis, Texas A&M University, College Station, TX (1987).
28. C. A. Vincent, "Modern Batteries," Edward Arnold Ltd., London, UK (1984).
29. D. C. Melnik, "Expanded Lead Grids for Batteries," Report on seminar, Lead Development Association, London, UK (January 1981).

I-BIEM. An Iterative Boundary Integral Equation Method for Computer Solutions of Current Distribution Problems with Complex Boundaries—A New Algorithm

I. Theoretical

B. D. Cahan* and Daniel Scherson*

Case Center for Electrochemical Sciences and the Department of Chemistry, Case Western Reserve University, Cleveland, Ohio 44106

Margaret A. Reid*

Case Center for Electrochemical Sciences and the Department of Chemistry, Case Western University, Cleveland, Ohio 44106 and NASA Lewis Research Center, Cleveland, Ohio 44135

ABSTRACT

A new algorithm for an iterative computation of solutions of Laplace's or Poisson's equations in two dimensions using Green's second identity is presented. This algorithm converges strongly and geometrically and can be applied to curved, irregular, or moving boundaries with nonlinear and/or discontinuous boundary conditions. It has been implemented in Pascal on a number of micro- and minicomputers and applied to several geometries. Cases with known analytic solutions have been tested. Convergence to within 0.1% to 0.01% of the theoretical values are obtained in a few minutes on a microcomputer.

The evaluation of current and potential distributions in configurations similar to those found in actual electrochemical applications can be difficult at best. Those configurations for which analytic solutions exist often derive from the field of heat flow and almost universally invoke linear or linearized boundary conditions. A wide variety of techniques for computer solutions of these problems can be found in the literature (1). Computer simulations often involve finite element or finite difference calculations over a regular grid, often rectilinear or square, although other grids have been used to match nonrectangular boundaries. Another technique which has been used for some geometries where it is applicable has been to find a Green's function for the problem. This involves finding a function [which may be analytic or a fitted polynomial in terms of, *e.g.*, Bessel functions (2) or B-spline functions (3)] which satisfies Laplace's equation for a given set of boundary conditions. Finding this function often requires a good deal of mathematical intuition, and a separate function must be derived or developed for each case.

One of the more popular methods, the finite difference method (FDM), involves a relaxation network technique in which a domain is simulated with a discrete grid and the values at the points are systematically and repeatedly replaced with the average of their neighbors using a version of the mean value theorem that is discrete. For a resolution of $1/n$ of the domain size, arrays of the orders of n^2 points must be used for a two-dimensional problem. The FDM is easily understood and can be readily implemented on a small computer at low resolution. With even a moder-

*Electrochemical Society Active Member.